Underwater Acoustic Channel Estimation via Complex Homotopy

Chenhao Qi*, Lenan Wu*, and Xiaodong Wang†
*Key Laboratory of Underwater Acoustic Signal Processing of Ministry of Education
School of Information Science and Engineering, Southeast University, Nanjing 210096, China
†Department of Electrical Engineering, Columbia University, New York, NY 10027
Email: qch@seu.edu.cn

***Abstract*—Underwater acoustic (UWA) channel is typically sparse. In this paper, a complex Homotopy algorithm is presented and then applied for UWA OFDM channel estimation. Two enhancements that exploit UWA channel temporal correlation for the compressed-sensing(CS)-based channel estimators are proposed. The first one is based on a first-order Gauss-Markov (GM) model which uses the previous channel estimate to assist current one. The other is to use the recursive least-squares (RLS) algorithm together with the CS algorithms to track the time-varying UWA channel. Simulation results show that the Homotopy algorithm offers faster and more accurate UWA channel estimation performance than other sparse recovery methods, and the proposed enhancements offer further performance improvement.**

***Index Terms*—Underwater acoustic (UWA) channel, channel estimation, sparse recovery, Homotopy**

I. Introduction

Underwater acoustic (UWA) channel is a fast time-varying multipath sparse channel with large delay spread. The channel impulse response (CIR) is usually dominated by a small number of significant paths, resulting in most of the channel coefficients are either zero or nearly zero [1]. Recently, compressed sensing (CS) that enables efficient reconstruction of sparse signals from relatively few linear measurements has been applied for UWA channel estimation [2], [3]. Many CS algorithms including matching pursuit (MP), orthogonal matching pursuit (OMP) and basis pursuit (BP) have been studied of intensive interest for UWA OFDM systems [4], [5]. In particular, BP is demonstrated to outperform OMP especially for severe Doppler spread conditions [4]. In [5], three BP algorithms including ℓ_1-LS, YALL1 and SpaRSA are compared. However, the complexity of BP algorithms is much higher than that of OMP. Considering the fact that the channel estimates have to be frequently updated in UWA communications, it's computationally expensive to apply BP for real-time UWA channel estimation. It's necessary to explore alternative high-performance and lower-complexity CS algorithms.

In this paper, we apply the Homotopy algorithm for UWA channel estimation. We first extend the original Homotopy algorithm that is only for real-valued signals to the complex field, due to the fact that in practice the channel taps of each path are usually complex-valued. Then two enhancements that exploit the channel temporal correlation are proposed for the CS-based channel estimators. The first one is to use a first-order Gauss-Markov (GM) model and take advantage of previous channel estimate to assist current estimation. The other is to use the recursive least-squares (RLS) algorithm together with the sparse recovery to track the time-varying UWA channel.

The notation used in this paper is according to the convention. Symbols for matrices (upper case) and vectors (lower case) are in boldface. $(\cdot)^T$, $(\cdot)^H$, $|\cdot|$, $\|\cdot\|_1$ $\|\cdot\|_2$, $\mathbb{C}$, $\mathbb{R}$, $diag\{\cdot\}$, $\boldsymbol{I}_L$, $\mathbf{0}_{M\times N}$, $\Re$, $\Im$ and $\mathcal{CN}$ denote transpose, conjugate transpose (Hermitian), absolute value, ℓ_1-norm, ℓ_2-norm, the set of complex number, the set of real number, the diagonal matrix, the identity matrix with dimension L, the M by N zero matrix, the real part, the imaginary part and the complex Gaussian distribution, respectively. $O(\cdot)$ means the order. $\hat{\phi}$ denotes the estimate of the parameter of interest ϕ.

II. System Descriptions

We consider the UWA channel that has a time-varying multipath CIR

$$h(\tau,t)=\sum_{i=1}^{S}\alpha_i(t)\delta(\tau-\tau_i(t)) \tag{1}$$

where S, $\alpha_i(t)$ and $\tau_i(t)$ are the number of total paths, the i-th path attenuation and the path delay, respectively. Supposing the dominant Doppler shift is caused by the relative movement between the transmitter and the receiver [6], all paths have the similar Doppler scaling factor $\varepsilon(t)$ such that $\tau_i(t)\approx\tau_i-\varepsilon(t)t$. Let $s(t)=\mathrm{Re}\{x(t)e^{j2\pi f_c t}\}$ denote the transmitted signal in passband, where f_c is the carrier frequency and $x(t)$ is the baseband OFDM signal. Within the duration of each OFDM packet, the parameters are treated as constants since the coherence time of UWA channel is usually on the order of seconds while each OFDM packet is no more than hundreds of milliseconds [2]. Then the received passband signal is

$$r(t)=\mathrm{Re}\left\{\sum_{i=1}^{S}\alpha_i x\Big((1+\varepsilon)t-\tau_i\Big)e^{j2\pi f_c\left((1+\varepsilon)t-\tau_i\right)}\right\}+n(t) \tag{2}$$

where $n(t)$ is the additive Gaussian noise. We notice that it is scaled in time by $1/(1+\varepsilon)$ and the Doppler shift $e^{j2\pi f_c\varepsilon t}$ is frequency-dependent. Since the bandwidth is comparable with

978-1-4577-2053-6/12/$31.00 ©2012 IEEE

the carrier frequency in UWA communications, the Doppler shift cannot be regarded as the same for the whole band. Here we adopt a two-step approach proposed in [6] to mitigate the Doppler effect. The first step is resampling and the second is the carrier frequency offset (CFO) compensation. Each OFDM packet contains one preamble and one postamble, i.e., linear frequency modulated (LFM) waveforms. By cross-correlating the received signal with the known preamble and postamble, the receiver estimates the length of each OFDM packet and obtains an estimated Doppler scaling factor $\hat{\varepsilon}$. As the frequency range used for UWA communications is usually tens of thousands of hertz, we can directly sample the received passband signal without down conversion. The equivalent received baseband signal after resampling is

$$y(t) = \sum_{i=1}^{S} \alpha_i x\left(\frac{1+\varepsilon}{1+\hat{\varepsilon}}t - \tau_i\right) e^{j2\pi f_c\left(\frac{\varepsilon-\hat{\varepsilon}}{1+\hat{\varepsilon}}t-\tau_i\right)} + n_B(t) \tag{3}$$

where $n_B(t)$ is the equivalent baseband noise. We define the residual CFO as

$$f_o = \frac{\varepsilon - \hat{\varepsilon}}{1+\hat{\varepsilon}} f_c \tag{4}$$

which is assumed to be uniformly distributed over the whole bandwidth [6]. Therefore, a wideband system is converted into a narrow band system with frequency-independent CFO. Then We can apply the well-developed null-subcarrier-based scheme for CFO compensation. More discussions on the residue CFO are found in [4] where the inter-channel interference (ICI) is also considered.

Due to the large delay spread of UWA channel, we prefer ZP-OFDM to CP-OFDM [7]. ZP-OFDM saves the transmission energy by zero-padding (ZP) rather than filling cyclic prefix (CP). Considering a ZP-OFDM system, there are totally N_d subcarriers, among which N_p ($N_p \le N_d$) are selected as pilots, with positions $1 \le k_1 < k_2 < \cdots < k_{N_p} \le N_d$, and N_u null subcarriers are used for CFO compensation. We denote the transmitted pilots and the received pilots as $X(k_1), X(k_2), \cdots, X(k_{N_p})$ and $Y(k_1), Y(k_2), \cdots, Y(k_{N_p})$, respectively. Considering a UWA channel whose CIR length after sampling is L, we have

$$\boldsymbol{y} = \boldsymbol{A}\boldsymbol{h} + \boldsymbol{\eta} \tag{5}$$

where $\boldsymbol{A} = \boldsymbol{X}\boldsymbol{F}_{N_p \times L}$, $\boldsymbol{X} = diag\left\{X(k_1), X(k_2), \cdots, X(k_{N_p})\right\}$, $\boldsymbol{F}_{N_p \times L}$ is a submatrix selected by the row indices $[k_1, k_2, \cdots, k_{N_p}]$ and column indices $[0, 1, \cdots, L-1]$ from the standard $N_d \times N_d$ Fourier matrix, $\boldsymbol{y} = [Y(k_1), Y(k_2), \cdots, Y(k_{N_p})]^{\mathrm{T}}$, $\boldsymbol{h} = [h(0), h(1), \cdots, h(L-1)]^{\mathrm{T}}$, and $\boldsymbol{\eta} = [\eta(0), \eta(1), \cdots, \eta(N_p-1)]^{\mathrm{T}} \sim \mathcal{CN}(\boldsymbol{0}, \sigma_\eta^2 \boldsymbol{I}_{N_p})$.

Since the system sampling interval is much smaller compared to the channel delay spread, most channel coefficients are either zero or nearly zero, which means that $\boldsymbol{h}$ is a sparse vector. We suppose $\boldsymbol{h} \in \mathbb{R}^L$ has S non-zero components, with $S \ll L$. If $\boldsymbol{A}$ has more rows than columns ($N_p > L$), then (5) is a standard least-squares (LS) problem. However, we are more interested in the sparse case ($N_p < L$), where the number of pilots is smaller than the number of channel coefficients.

III. Channel Estimation via Complex Homotopy

The sparse recovery algorithms can be roughly divided into two classes, including the convex optimization algorithms, i.e., ℓ_1-LS [8], YALL1 [5], SpaRSA [9], and the greedy algorithms, i.e., MP, OMP [10], CoSaMP [11], subspace pursuit (SP) [12] and Homotopy [13]. Since frequent channel estimation is required in UWA communications, low-complexity greedy algorithms are much preferred. Among the many greedy algorithms, CoSaMP and SP require explicit knowledge of the sparsity. MP and OMP have been extensively studied with their variants [14], [15]; and it is known that they may not always achieve satisfactory performance [16]. In [13] it is shown that Homotopy has the same order of complexity as OMP while its sparse recovery performance is as good as that obtained from convex optimization.

A. Complex Homotopy

Real-valued Homotopy is proposed in [13] as a least angle regression (LARS) [17] algorithm with the least absolute shrinkage and selection operator (LASSO) modifications. After greedily selecting the first column based on the maximum-inner-product rule and adding it to the current column selection as MP and OMP, Homotopy steps forward until one column outside the selection appears to have the same inner product with the current residue as the columns inside the selection. Then the column is selected and a new step along an equiangular direction having the same inner product with all vectors in the selection is updated. The iteration is repeated until the stop condition is satisfied. Unlike MP and OMP removing all the projective components at each iteration, Homotopy only removes part of it, whose value actually equals the step size at each iteration. Once it eliminates the superiority of the maximal-inner-product column over other columns, Homotopy fairly treats all the columns.

Since UWA channel is essentially sparse with complex-valued channel taps, we extend Homotopy from the real field to the complex field before applying for channel estimation. Note that unlike MP and OMP, for which the extension to the complex field is straightforward by simply replacing the transpose operator with the Hermitian operator, the extension of Homotopy to the complex field is more involved.

Considering the following unconstrained optimization problem

$$\min_{\boldsymbol{h}} \|\boldsymbol{y} - \boldsymbol{A}\boldsymbol{h}\|_2^2/2 + \lambda\|\boldsymbol{h}\|_1 \tag{6}$$

the theory for penalty functions implies that Homotopy starts at $\lambda \in \mathbb{R}$ large and $\boldsymbol{h} = 0$, and terminates when $\lambda \to 0$. Meanwhile $\boldsymbol{h}$ converges to the solution of the noiseless sparse recovery problem

$$\min_{\boldsymbol{h}} \|\boldsymbol{h}\|_1 \text{ s.t. } \boldsymbol{y} = \boldsymbol{A}\boldsymbol{h} \tag{7}$$

For the noisy sparse recovery problem considered in this paper, the stop condition $\lambda \to 0$ should be replaced by

$$\|\boldsymbol{y} - \boldsymbol{A}\boldsymbol{h}\|_2 \le \sigma_\eta \tag{8}$$

Suppose the objective function to be

$$f_\lambda(\boldsymbol{h}) = \|\boldsymbol{y} - \boldsymbol{A}\boldsymbol{h}\|_2^2/2 + \lambda\|\boldsymbol{h}\|_1 \tag{9}$$

A necessary condition for $\boldsymbol{h}$ to be a minimizer of $f_\lambda(\boldsymbol{h})$ is that the subdifferential of $f_\lambda(\boldsymbol{h})$ is zero, denoted as

$$\partial f_\lambda(\boldsymbol{h}) = -\boldsymbol{A}^H(\boldsymbol{y} - \boldsymbol{A}\boldsymbol{h}) + \lambda\partial\|\boldsymbol{h}\|_1 = 0 \tag{10}$$

where the subdifferential $\partial\|\boldsymbol{h}\|_1$ of $\|\boldsymbol{h}\|_1$ is given by

$$\partial\|\boldsymbol{h}\|_1 = \left\{\boldsymbol{\omega} \in \mathbb{C}^L \;\middle|\; \begin{array}{ll} \omega(i) = \frac{h(i)}{|h(i)|}, & h(i) \neq 0 \\ \omega(i) = \{x \in \mathbb{C}, |x| \leq 1\}, & h(i) = 0 \end{array}\right\}$$

where $h(i)$ and $\omega(i)$ denote the i-th component of $\boldsymbol{h}$ and $\boldsymbol{\omega}$, respectively. Let

$$T = \{i \;\big|\; h(i) \neq 0\}$$

denote the support of $\boldsymbol{h}$ and

$$\boldsymbol{c} = \boldsymbol{A}^H(\boldsymbol{y} - \boldsymbol{A}\boldsymbol{h})$$

denote the correlations between the dictionary matrix and the residue. Then $\partial f_\lambda(\boldsymbol{h}) = 0$ can be equivalently written as two conditions

$$\left\{\begin{array}{lcl} \boldsymbol{c}(T) & = & \lambda \cdot \frac{\boldsymbol{h}(T)}{|\boldsymbol{h}(T)|} \\ |\boldsymbol{c}(T^c)| & \leq & \lambda \end{array}\right. \tag{11}$$

where T^c, $\boldsymbol{c}(T)$ and $\boldsymbol{h}(T)$ denote the complement of T, the correlations on the support T and the channel parameters on T, respectively. Homotopy traces a solution path by maintaining these two conditions.

In order to clarify the notation, we use subscript l to represent the parameters at l-th step. We initialize the parameters to be

$$\boldsymbol{c}_0 = \boldsymbol{A}^H\boldsymbol{y} \tag{12}$$

$$\lambda_0 = \max_{i\in\{1,\ldots,L\}} |\boldsymbol{c}_0(i)| \tag{13}$$

$$I_0 = \arg\max_{i\in\{1,\ldots,L\}} |\boldsymbol{c}_0(i)| \tag{14}$$

At the l-th step, an update direction $\boldsymbol{d}_l \in \mathbb{C}^L$ is first computed by solving

$$\boldsymbol{A}^H(I_l)\boldsymbol{A}(I_l)\boldsymbol{d}_l(I_l) = \frac{\boldsymbol{c}_l(I_l)}{\lambda_l} \tag{15}$$

The components of $\boldsymbol{d}_l$ outside I_l are set zero. Next, we figure out the step size γ_l so that a new solution at the $(l+1)$-th step can be obtained as

$$\boldsymbol{h}_{l+1} = \boldsymbol{h}_l + \gamma_l\boldsymbol{d}_l \tag{16}$$

where $\boldsymbol{h}_l \in \mathbb{C}^L$ is initialized to be a zero vector and converges to the solution of (6). We have

$$\begin{array}{rcl} \boldsymbol{c}_{l+1} & = & \boldsymbol{A}^H(\boldsymbol{y} - \boldsymbol{A}\boldsymbol{h}_{l+1}) \\ & = & \boldsymbol{A}^H(\boldsymbol{y} - \boldsymbol{A}\boldsymbol{h}_l) - \gamma_l\boldsymbol{A}^H\boldsymbol{A}\boldsymbol{d}_l \\ & = & \boldsymbol{c}_l - \gamma_l\boldsymbol{A}^H\boldsymbol{A}\boldsymbol{d}_l \end{array} \tag{17}$$

Since current selected columns always follow (11), we have

$$\boldsymbol{c}_{l+1}(I_l) = (\lambda_l - \gamma_l)\frac{\boldsymbol{h}_l(I_l)}{|\boldsymbol{h}_l(I_l)|} \tag{18}$$

On the other hand, we want to find a new column from I_l^c for the $(l+1)$-th step, denoted as

$$\boldsymbol{c}_{l+1}(I_l^c) = \boldsymbol{c}_l(I_l^c) - \gamma_l d\boldsymbol{\mu}(I_l^c) \tag{19}$$

where we define

$$\boldsymbol{c}_l(I_l^c) = \boldsymbol{A}^H(I_l^c)(\boldsymbol{y} - \boldsymbol{A}\boldsymbol{h}_l)$$

$$d\boldsymbol{\mu}(I_l^c) = \boldsymbol{A}^H(I_l^c)\boldsymbol{A}\boldsymbol{d}_l$$

Once a column in I_l^c appears to have the same projection as the columns in I_l, which actually occurs when (18) equals (19) in amplitude as

$$\left|\boldsymbol{c}_l(i) - \gamma_l d\boldsymbol{\mu}(i)\right| = \lambda_l - \gamma_l,\;\; i \in I_l^c \tag{20}$$

we consider it to be one possible candidate for the next selection because the residue can decline equally in this direction. We further define

$$c_R = \Re\left\{\boldsymbol{c}_l(i)\right\}, \quad c_I = \Im\left\{\boldsymbol{c}_l(i)\right\}$$

$$\mu_R = \Re\left\{d\boldsymbol{\mu}(i)\right\}, \quad \mu_I = \Im\left\{d\boldsymbol{\mu}(i)\right\}$$

and then get a quadratic equation as

$$(\mu_R^2 + \mu_I^2 - 1)\gamma_l^2 + 2(\lambda_l - c_R\mu_R - c_I\mu_I)\gamma_l + c_R^2 + c_I^2 - \lambda_l^2 = 0 \tag{21}$$

We figure out two roots and select the smaller one, denoted as $\gamma(i)$, among which we select

$$\gamma_l^+ = \min_{i\in I_l^c}\{\gamma(i)\} \tag{22}$$

Moreover, the selection of the breakpoint in the solution path for the complex Homotopy should also be extended. The breakpoint occurs when one component of $\boldsymbol{h}_l(I_l)$ crosses zero, which means both the real part and imaginary part equal zero. If

$$I_s = \left\{ i \in I_l \;\middle|\; \frac{\Re\left\{\boldsymbol{h}_l(i)\right\}}{\Re\left\{\boldsymbol{d}_l(i)\right\}} = \frac{\Im\left\{\boldsymbol{h}_l(i)\right\}}{\Im\left\{\boldsymbol{d}_l(i)\right\}} \right\} \neq \varnothing$$

then

$$\gamma_l^- = \min_{i\in I_s}\left\{ -\frac{\Re\left\{\boldsymbol{h}_l(i)\right\}}{\Re\left\{\boldsymbol{d}_l(i)\right\}} \right\} \tag{23}$$

Finally the step size γ_l is determined to be the minimum between γ_l^+ and γ_l^- if γ_l^- exists. We use (16) to update the solution $\boldsymbol{h}_{l+1}$. If $\gamma_l = \gamma_l^+$, we add a new column indicated by γ_l^+ into I_l and get I_{l+1}. If $\gamma_l = \gamma_l^-$, we delete the column indicated by γ_l^- from I_l and get I_{l+1}. We also update $\lambda_{l+1} = \lambda_l - \gamma_l$. These steps are repeated until the stop condition (8) is satisfied.

The above extension to the complex field can be easily verified by forcing $c_I = 0$, $\mu_I = 0$ in (21), which then reduces to the real-field form of Homotopy [13]. Unlike OMP removing the whole projection at each step, Homotopy only removes part of it, which can be thought as a moderate greedy algorithm. Moreover, Homotopy allows the columns to enter as well as to leave the current selection, which makes it more powerful than OMP. In terms of computational complexity, Homotopy is roughly in the same order as OMP with $O(N_p^2L)$ while the convex optimization algorithms are about $O(L^3)$.

B. Incorporating Channel Temporal Correlation

The basic idea is to use the channel estimate $\boldsymbol{h}^{(m-1)}$ from the previous time slot $(m-1)$ to assist the current channel estimate $\boldsymbol{h}^{(m)}$. Since the UWA channel is temporally correlated, we model it using a simple first-order Gauss-Markov (GM) process, given by

$$\begin{aligned} \boldsymbol{h}^{(m)} &= \kappa \boldsymbol{h}^{(m-1)} + \boldsymbol{v}^{(m)} && (24) \\ \text{with} \quad \kappa &= J_0(2\pi f_d T_s) && (25) \end{aligned}$$

where J_0, f_d and T_s denote the zero order Bessel function of the first kind, the maximum Doppler shift and the symbol period, respectively. $\boldsymbol{v}^{(m)} \sim \mathcal{CN}(\boldsymbol{0}, \sigma_v^2 \boldsymbol{I}_L)$ is a Gaussian noise term independent of $\boldsymbol{h}^{(m-1)}$. We rewrite (5) as

$$\boldsymbol{y}^{(m)} = \boldsymbol{A}\boldsymbol{h}^{(m)} + \boldsymbol{\eta}^{(m)} \tag{26}$$

Combining (24) and (26) using matrix notation we have

$$\begin{bmatrix} \boldsymbol{y}^{(m)} \\ \kappa \boldsymbol{h}^{(m-1)} \end{bmatrix} = \begin{bmatrix} \boldsymbol{A} \\ \boldsymbol{I_L} \end{bmatrix} \boldsymbol{h}^{(m)} + \begin{bmatrix} \boldsymbol{\eta}^{(m)} \\ -\boldsymbol{v}^{(m)} \end{bmatrix} \tag{27}$$

Obviously we can still apply the sparse recovery algorithms to solve $\boldsymbol{h}^{(m)}$ with the following two stopping conditions

$$\begin{aligned} \|\boldsymbol{y}^{(m)} - \boldsymbol{A}\boldsymbol{h}^{(m)}\|_2 &\leq \sigma_\eta && (28) \\ \text{and} \quad \|\boldsymbol{h}^{(m)} - \kappa \boldsymbol{h}^{(m-1)}\|_2 &\leq \sigma_v && (29) \end{aligned}$$

At low signal-to-noise ratio (SNR) where σ_η is comparable to σ_v, (27) can be regarded as having additional observations compared to (26), where improved channel estimation performance is expected.

C. Channel Tracking via Recursive Least-Squares (RLS)

The RLS algorithm is widely used for tracking time-varying processes. Here we consider further improving the UWA channel estimation by integrating the RLS algorithm. In particular, we modify the objective function (6) as

$$\min_{\boldsymbol{h}^{(m)}} \sum_{i=i_0}^{m} \beta^{m-i} \left\| \boldsymbol{y}^{(i)} - \boldsymbol{A}\boldsymbol{h}^{(m)} \right\|_2^2 / 2 + \lambda^{(m)} \left\| \boldsymbol{h}^{(m)} \right\|_1 \tag{30}$$

where i_0 and m are the starting and ending point of the weighted window, respectively. m is the current time point where the channel is to be estimated. $\beta \in [0, 1)$ is the forgetting factor chosen to tradeoff between the convergence speed and the performance. Correspondingly, (9) and (10) are modified as

$$f_{\lambda^{(m)}}\left(\boldsymbol{h}^{(m)}\right) = \sum_{i=i_0}^{m} \beta^{m-i} \left\| \boldsymbol{y}^{(i)} - \boldsymbol{A}\boldsymbol{h}^{(m)} \right\|_2^2 / 2 + \lambda^{(m)} \left\| \boldsymbol{h}^{(m)} \right\|_1$$

and

$$\partial f_{\lambda^{(m)}}\left(\boldsymbol{h}^{(m)}\right) = -\boldsymbol{A}^H \Big(\sum_{i=i_0}^{m} \beta^{m-i} \boldsymbol{y}^{(i)} - \boldsymbol{A} \sum_{i=i_0}^{m} \beta^{m-i} \boldsymbol{h}^{(m)} \Big) + \lambda^{(m)} \partial \left\| \boldsymbol{h}^{(m)} \right\|_1$$

respectively. We define

$$\boldsymbol{c}^{(m)} = \boldsymbol{A}^H \Big(\frac{1-\beta}{1-\beta^m} \sum_{i=i_0}^{m} \beta^{m-i} \boldsymbol{y}^{(i)} - \boldsymbol{A}\boldsymbol{h}^{(m)} \Big) \tag{31}$$

Then (11) is modified as

$$\begin{cases} \boldsymbol{c}^{(m)}(T) &= \frac{(1-\beta)\lambda^{(m)}}{1-\beta^m} \cdot \frac{\boldsymbol{h}^{(m)}(T)}{|\boldsymbol{h}^{(m)}(T)|} \\ |\boldsymbol{c}^{(m)}(T^c)| &\leq \frac{(1-\beta)\lambda^{(m)}}{1-\beta^m} \end{cases} \tag{32}$$

We can apply complex Homotopy by substituting $\boldsymbol{y}$ and λ in (6) with

$$\begin{aligned} \boldsymbol{z}^{(m)} &= \frac{1-\beta}{1-\beta^m} \sum_{i=i_0}^{m} \beta^{m-i} \boldsymbol{y}^{(i)} && (33) \\ \text{and} \quad \xi &= \frac{(1-\beta)\lambda^{(m)}}{1-\beta^m} && (34) \end{aligned}$$

respectively. The iterative procedure for updating (33) becomes

$$\boldsymbol{z}^{(m)} = \frac{\beta - \beta^m}{1-\beta^m} \boldsymbol{z}^{(m-1)} + \frac{1-\beta}{1-\beta^m} \boldsymbol{y}^{(m)} \tag{35}$$

Similarly we can integrate the RLS algorithm with other sparse recovery algorithms such as OMP and YALL1. The performance improvement by the RLS weighted sparse recovery is determined by β and i_0. For rapid time-varying UWA channels, we set β small and control the weighted window length by setting i_0 close to m; while for relatively slowly time-varying UWA channels, we choose β close to 1 and increase $m - i_0$.

IV. Simulation Results

Three BP algorithms as ℓ_1-LS, SpaRSA and YALL1 are compared in [5] where YALL1 and SpaRSA are concluded to be the better than OMP. So in this section we compare Homotopy with YALL1 as well as OMP. We use the following sparse multipath channel model

$$c(\tau) = \sum_{i=1}^{S} a_i \delta(\tau - \tau_i)$$

to obtain channel realizations. $\{a_i\} \sim \mathcal{CN}(\boldsymbol{0}, e^{-b\tau_i} \boldsymbol{I}_S)$. $b = 1/16$ is the exponential power delay profile and τ_i is the delay spread for the i-th path [18]. In practice, we may replace the simulated channel realizations with the real UWA channel measurement data, if they are available. And it is verified in [4] that the simulations usually give the same performance trend as the real UWA experiments.

The parameters used in our simulations are listed in Table 1. The bandwidth $B = 4$kHz is centered around $f_c = 24$Hz and divided into $N_d = 512$ OFDM subcarriers, among which $N_p = 20$ and $N_u = 110$ are used for pilots and null subcarriers, respectively. The length of the guard interval is $N_G = 64$. A five-path ($S = 5$) channel with the maximum channel delay spread $L = 50$ is considered. According to [4], mild Doppler spread with the velocity standard deviation $\sigma_\upsilon = 0.1$ is assumed, which results in the Doppler spread at f_c to be around 2.7Hz.

We use random pilot placement according to the restricted isometry property (RIP) [19] and compare Homotopy, OMP and YALL1 with RLS and GM enhanced counterparts, as shown in Fig. 1. The MSE of Homotopy is better than that of

TABLE I
PARAMETERS OF THE SIMULATION.

Number of total subcarriers	$N_d = 512$
Number of null subcarriers	$N_u = 110$
Number of pilot subcarriers	$N_p = 20$
Length of zero padding	$N_G = 64$
Number of multipaths	$S = 5$
Length of CIR	$L = 50$
Carrier frequency	$f_c = 24$kHz
Signal bandwidth	$B = 4$kHz
Doppler spread at f_c	2.7Hz

OMP, especially for SNR > 25dB. Homotopy and YALL1 are not much different. We combine the advantages of the first-order GM model and the RLS weighted sparse recovery, which is denoted in brief as RLS CS with GM. We set the forgetting factor $\beta = 0.992$ and weighted window length $m - i_0 = 12$. It's observed from Fig. 1 that RLS Homotopy with GM performs better than RLS OMP with GM. RLS YALL1 is inferior to the above two since the GM model cannot be incorporated into the YALL1 solver.

The complexities of these algorithms are compared in terms of the CPU running time. The experiments are performed using MATLAB v7.9 (R2009b) running on a Lenovo laptop with an Intel Core 2 Duo CPU at 2.5GHz and 2GB of memory. SNR is fixed to be 30dB. We observe that Homotopy takes about 0.563s(seconds), which is similar to 0.526s of OMP and much lower than 2.313s of YALL1. RLS Homotopy with GM is about 0.02s higher than Homotopy.

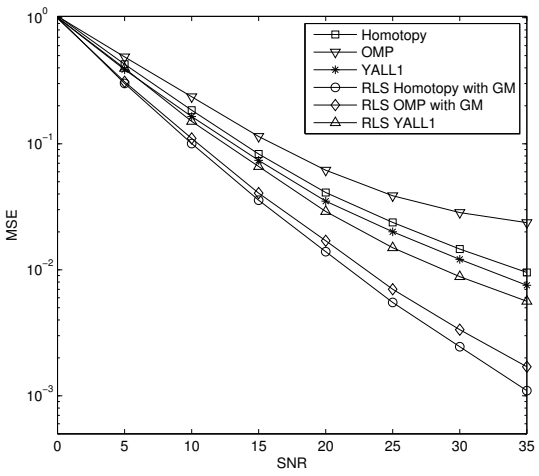

Fig. 1. Performance of different CS algorithms with GM and RLS.

V. CONCLUSIONS

We have investigated UWA OFDM channel estimation via complex Homotopy. We have proposed two enhancements to exploit the temporal correlation of UWA channel, including a first-order GM model and the RLS algorithm to track the time-varying UWA channel. Simulation results show that the proposed Homotopy algorithm together with the GM model and RLS tracking offers substantial performance improvement compared with the state-of-the-art UWA channel estimators.

ACKNOWLEDGMENT

The work is supported by the National Natural Science Foundation of China (NSFC) under the Grant 60872075, the Scientific Research Foundation of Southeast University under the Grant Seucx201116, Huawei Innovative Research Plan and CAST 8804009011.

REFERENCES

[1] M. Stojanovic and J. Preisig, "Underwater acoustic communication channels: Propagation models and statistical characterization," *IEEE Comm. Mag.*, vol. 47, no. 1, pp. 84–89, Jan. 2009.

[2] C. R. Berger, Z. Wang, J. Huang, and S. Zhou, "Application of compressive sensing to sparse channel estimation," *IEEE Comm. Mag.*, vol. 48, no. 11, pp. 164–174, Nov. 2010.

[3] W. U. Bajwa, J. Haupt, A. M. Sayeed, and R. Nowak, "Compressed channel sensing: A new approach to estimating sparse multipath channels," *Proceeds of the IEEE*, vol. 98, no. 6, pp. 1058–1076, June 2010.

[4] C. R. Berger, S. Zhou, J. C. Preisig, and P. Willett, "Sparse channel estimation for multicarrier underwater acoustic communication: From subspace methods to compressed sensing," *IEEE Trans. Sig. Proc.*, vol. 58, no. 3, pp. 1708–1721, Mar. 2010.

[5] J. Z. Huang, C. R. Berger, S. Zhou, and J. Huang, "Comparison of basis pursuit algorithms for sparse channel estimation in underwater acoustic OFDM," in *Proc. MTS/IEEE OCEANS*, Sydney, Australia, May 2010, pp. 1–6.

[6] B. Li, S. Zhou, M. Stojanovic, L. Freitag, and P. Willett, "Multicarrier communication over underwater acoustic channels with nonuniform Doppler shifts," *IEEE J. Ocean. Eng.*, vol. 33, no. 2, pp. 198–209, Apr. 2008.

[7] B. Li, S. Zhou, M. Stojanovic, and L. Freitag, "Pilot-tone based ZP-OFDM demodulation for an underwater acoustic channel," in *Proc. MTS/IEEE OCEANS*, Boston, MA, USA, Sept. 2006, pp. 1–5.

[8] S.-J. Kim, K. Koh, M. Lustig, S. Boyd, and D. Gorinevsky, "An interiorpoint method for large-scale ℓ_1-regularized least squares," *IEEE Trans. Sig. Proc.*, vol. 1, no. 4, pp. 606–617, Dec. 2007.

[9] S. J. Wright, R. D. Nowak, and M. A. T. Figueiredo, "Sparse reconstruction by separable approximation," *IEEE Trans. Sig. Proc.*, vol. 57, no. 7, pp. 2479–2493, July 2009.

[10] J. A. Tropp and A. C. Gilbert, "Signal recovery from random measurements via orthogonal matching pursuit," *IEEE Trans. Inf. Theory*, vol. 53, no. 12, pp. 4655–4666, Dec. 2007.

[11] D. Needell and J. A. Tropp, "CoSaMP: Iterative signal recovery from incomplete and inaccurate samples," *Applied and Computational Harmonic Analysis*, vol. 26, no. 3, pp. 301–321, Apr. 2008.

[12] W. Dai and O. Milenkovic, "Subspace pursuit for compressive sensing signal reconstruction," *IEEE Trans. Inf. Theory*, vol. 55, no. 5, pp. 2230–2249, May 2009.

[13] D. L. Donoho and Y. Tsaig, "Fast solution of ℓ_1-norm minimization problems when the solution may be sparse," *IEEE Trans. Inf. Theory*, vol. 54, no. 11, pp. 4798–4812, Nov. 2008.

[14] L. R. Neira and D. Lowe, "Optimized orthogonal matching pursuit approach," *IEEE Sig. Proc. Lett.*, vol. 9, no. 4, pp. 137–140, Apr. 2002.

[15] M. Andrle, L. R. Neira, and E. Sagianos, "Backward-optimized orthogonal matching pursuit approach," *IEEE Sig. Proc. Lett.*, vol. 11, no. 9, pp. 705–708, Sept. 2004.

[16] Y. Jin and B. D. Rao, "Performance limits of matching pursuit algorithms," in *Proc. ISIT*, Toronto, Canada, July 2008, pp. 2444–2448.

[17] B. Efron, T. Hastie, I. Johnstone, and R. Tibshirani, "Least angle regression," *Ann. Statist.*, vol. 32, no. 2, pp. 407–499, June 2004.

[18] M. R. Raghavendra and K. Giridhar, "Improving channel estimation in OFDM systems for sparse multipath channels," *IEEE Sig. Proc. Lett.*, vol. 12, no. 1, pp. 52–55, Jan. 2005.

[19] E. J. Candes and T. Tao, "Decoding by linear programming," *IEEE Trans. Inf. Theory*, vol. 51, no. 12, pp. 4203–4215, Dec. 2005.